海洋科学技術センター試験研究報告　第40号　JAMSTECR, 40（February 2000）

Development of a two-way nesting code for the Princeton Ocean Model

Yasumasa MIYAZAWA＊1
Shinya MINATO＊2

We developed a two-way nesting code for the Princeton Ocean Model (POM). The nesting code can reduce computer resources by embedding finer resolution grids within a coarser grid. The nesting code is written in Fortran 77 and users can easily implement the nesting by inserting a few subroutines in the existing user's coarse grid POM code. In this paper the nesting algorithm is described and the some preliminary results are demonstrated. The validity of the nesting method is shown in the some problems such as unstable front, flow over a seamount and response of jet to strong wind stress.

Key Words : Princeton Ocean Model (POM), two-way nesting, coastal ocean modelling

プリンストン海洋モデルに対する双方向ネスティングコードの開発

宮澤　泰正＊3
湊　　信也＊4

プリンストン海洋モデル（ＰＯＭ）に対する双方向ネスティングコードを開発した。ネスティングコードは粗い格子により細かな格子をはめこむことによって計算資源の節約を可能にする。ネスティングコードはＦｏｒｔｒａｎ77言語で記述されていて，ユーザーは既存の粗格子ＰＯＭコードにいくつかのサブルーチンを挿入することにより容易にネスティングを実現できる。この論文ではネスティングアルゴリズムを説明し，初期的な結果を示す。不安定フロント，海山上の流れ，ジェットの強風に対する応答といった問題においてネスティングの有効性を示す。

キーワード：プリンストン海洋モデル（ＰＯＭ），双方向ネスティング，沿岸海岸モデリング

＊１　Frontier Research System for Global Change
＊２　Japan Meteorological Agency
＊３　地球フロンティア研究システム
＊４　気象庁

1 Introduction

Numerical ocean modelling has recently been developed toward realistic simulation or prediction (Kagimoto and Yamagata (1997)[1], Mitsudera et al. (1997)[2], Guo et al. (1999)[3]). The realistic numerical ocean modelling needs high resolution grid because of considerably smaller scale of the target phenomenon (e. g. Kuroshio meander, meso scale eddy, etc.) than the basin scale gyre circulation. Computer resources tend to be rich in recent years, but it is still important to develop methods that can magnify the particular region in wide model basin within the range of specified computer resources. Nesting of multi-resolution grids is effective to treat large scale phenomenon such and small scale phenomenon at the same time.

Nesting methods allow to reduce computer resources by embedding finer resolution grid within a coarser grid as well as the variable grid spacing or the curvilinear coordinate. We emphasize flexibilities of the nesting method compared with the other grid systems. The finer higher resolution grid can be embedded in favorite area of the existing coarse grid when this area becomes interesting for users, just like a microscope.

In weather predictions nesting methods have mainly been used (e. g. Kurihara and Bender (1980)[4]; Zhang et al. (1986)[5]). Nesting for ocean models have recently been attempted (Spall and Holland (1991)[6]; Oey and Chen (1993)[7]; Oey (1996)[8]). Guo et al. (1999)[3] have particularly begun to develop one-way nesting ocean model for the Japan Coastal Ocean Predictability Experiment (JCOPE). We independently developed a two-way nesting POM code mainly according to Oey and Chen (1992)[7]. Our nesting POM is applied to various ocean processes such as unstable front and meander, flow over a seamount, and response of jet to strong wind stress whose physical process is intensively investigated by Miyazawa and Minato (1999)[9]. We intend to provide the nesting code as one of options to simulate ocean circulation effectively.

There are two types of nesting, one-way type and two-way type. One-way nesting means that information of the coarse grid is only put on the boundary of the nested grid. On the other hand, two-way nesting means that information of the nested grid is additionally reflected on the coarse grid. Our nesting code has the both one-way and two-way options.

This paper is organized as follows. In section 2 the Princeton Ocean Model (POM) is briefly described and then the adopted nesting method is described.In section 3 some preliminary results of the nesting POM are presented. Applications to unstable front, flow over a seamount and response of jet to strong wind stress are demonstrated. We summarize results in section 4.

2 A nesting model for the Princeton Ocean Model

The Princeton Ocean Model (POM, Mellor (1996)[10]) is one of the three dimensional ocean circulation models and it is widely used for ocean modelling from the basin scale modelling (e. g. Kagimoto and Yamagata (1997)[1]; Mitsudera et al. (1997)[2]; Guo et al. (1999)[3]) to the coastal ocean modelling (e. g. Minato (1998)[11]; Hong (1998)[12]). This model uses the bottom following (sigma) coordinate and the horizontal Arakawa C-grid. It adopts the time splitting technique to solve two modes, that is two dimensional external mode for the free surface elevation and depth averaged velocities and three dimensional internal mode for the velocities and tracers (temperature and salinity). The leap-frog scheme is used as the time difference scheme and the Asselin filter (Asselin(1972)[13]) is applied to remove gap between the odd and even time steps. It also adopts the Mellor-Yamada's level 2.5 turbulence closure scheme (Mellor and Yamada (1982)[14]). The density is determined by the UNESCO equation of state, as adopted by Mellor (1991)[15].

The nesting algorithm for the POM is generally constructed according to Oey and Chen (1993)[7] and Oey (1996)[8]. The nesting POM code consists of coarse grid part, fine grid part and communication part between them. The coarse grid and the fine grid have different horizontal grid size (Δx_c, Δx_n, respectively) and same vertical resolution. The time splitting technique used in the POM forces us to use four different time steps (see Fig. 1) : first for the nested grid external mode Δt_{ne}, second for the coarse grid external mode Δt_{ce}, third for the nested grid internal mode Δt_{ni}, and fourth for the coarse grid internal mode Δt_{ci}, such that

$$M = \frac{\Delta x_c}{\Delta x_n} = \frac{\Delta t_{ce}}{\Delta t_{ne}} = \frac{\Delta t_{ci}}{\Delta t_{ni}} \tag{1}$$

where integer M is the nesting ratio. The coarse grid boundary values of the nested grid variables are specified on the input interface by bilinear interpolation (Fig. 2). Prognostic variables on the nested grid are time-stepped forward $M \cdot \Delta t_n$. The feedback step from the nested grid to the coarse grid in the two-way nesting is explained as follows. One of the model equation for the prognostic variable U is simply written, that is

$$\frac{\partial U}{\partial t} = X(U) + Z(U) \tag{2}$$

where $X(U)$ represents terms except for implicit vertical viscous/diffusion term $Z(U)$. We will refer to $X(U)$ as quasi-tendency term. Quasi-tendency terms X^n_{ijk} of the nested grid cell within one coarse grid cell (I, J, k) are averaged over on the nested grid $M \times M$ cells within the feedback interface shown in Fig. 2. Each original quasi-tendency term of the coarse grid variable is replaced with the new one (the averaged tendency terms within the feedback interface)

$$\left[X^c\left(U^c_{IJk}\right)_{IJk}\right]^{New} = \sum_{ij} W_{ij} X^n\left(U^n_{ijk}\right) \tag{3}$$

where W_{ij} is weight term for some kind of averaging. We

use the simple averaging such as

$$W_{ij} = \frac{1}{M \times M} \tag{4}$$

Then the prognostic variables on the coarse grid are time-stepped. The relationships between the coarse grid time-stepping and the fine grid time-stepping are shown in Fig. 1. The implicit calculations of vertical viscous/diffusion terms and the Asselin filtering are carried out in the coarse grid and the nested grid, separately.

Zhang et al. (1986)[5] pointed out that it is important to separate the input interface from the feedback interface. This procedure prevents from contamination of the information of the nested grid. We prepare somewhat wider area for the feedback interface of the external mode variables (Fig. 2). This procedure confirms the conservation of volume.

In the implementation nesting of the POM is easily realized by inserting a few subroutines for the nested grid calculation and those for communication between the coarse grid and the nested grid in the existing coarse grid code. We took care of minimization of code changes for the existing coarse grid code. The model variables are organized as three common blocks, namely, common block for the coarse grid, common block for the nested grid, common block for the communication part between the coarse grid and the nested grid. This allows a selection of the options of making load modules such as the coarse grid module or the nesting grid module. Inserting of subroutines for nesting is controlled by '#ifdef' actions. Our nesting POM code can be implemented on various workstations and PCs with standard Fortran 77 compilers. The described nesting algorithm is illustrated as a flow chart shown in Fig. 3.

Users can select 'interpolated topography' option or 'variable topography' option. This selection is accomplished by modification of two subroutines, 'MKGRID_F' and 'MKINIT_F' and addition of subroutine 'AJSTH_F' for 'variable topography' option (see Fig. 3). The 'interpolated topography' option allows interpolation of topography and initial condition of the nested grid from the coarse grid value. The 'variable topography' option allows new creation of the nested grid topography itself. The depth of coarse grid in the overlap region is adjusted so that it corresponding to the average of the nested grid depth. The initial condition of the nested grid is interpolated from the initial condition of the coarse grid so that it is consistent with topography of the nested grid. First the coarse grid value is transformed to z-coordinate value from sigma-coordinate value. The interpolation is carried out in z-coordinate grid and then the z-coordinate nested grid value is transformed to the sigma-coordinatenested grid value.

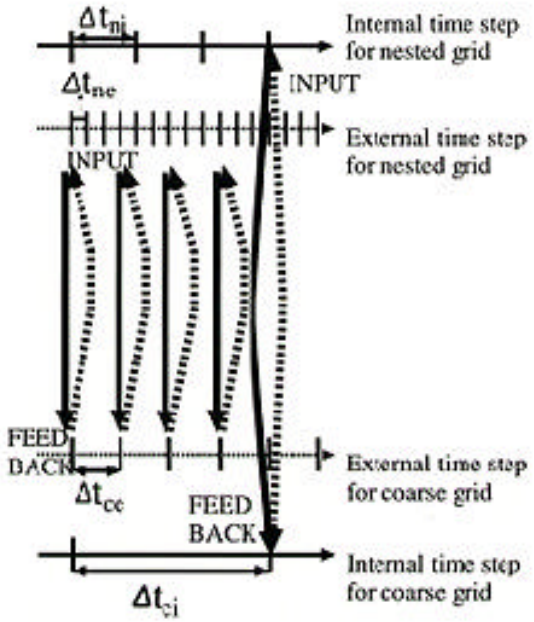

Fig. 1 Time-stepping in the coarse grid and the nested grid ratio 3:1

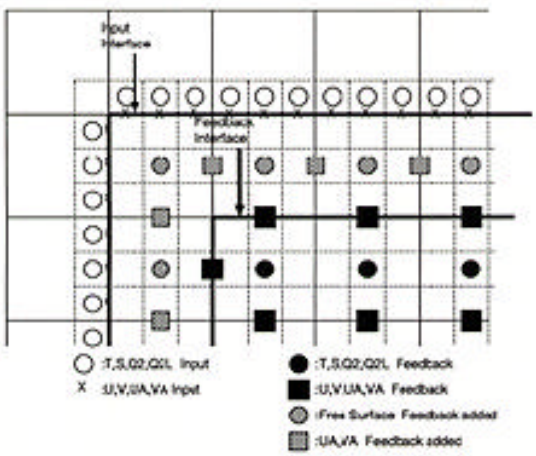

Fig. 2 The nasted grid system, grid ratio 3:1

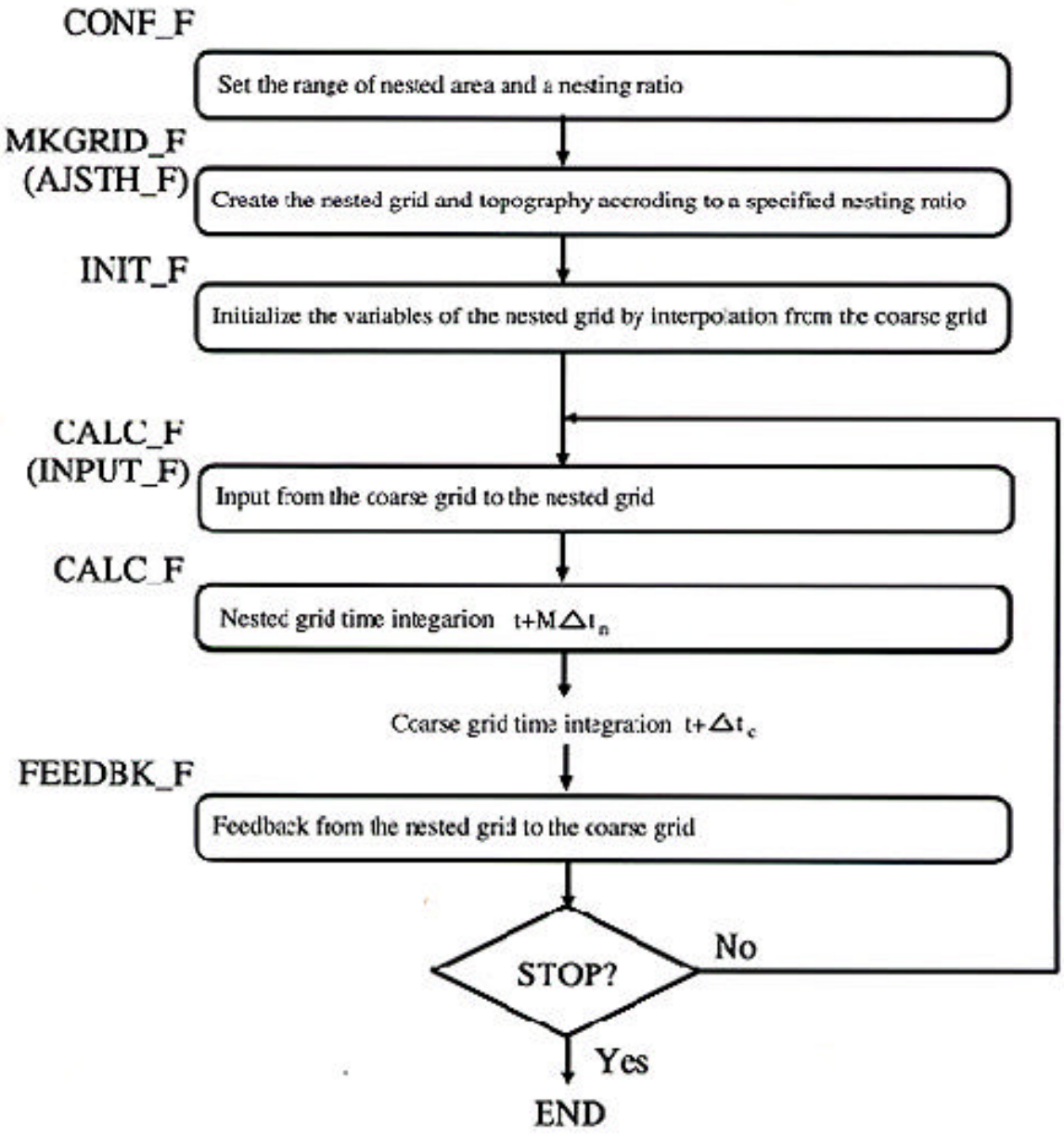

Fig. 3 Flow chart that consists of subroutines inserted in the coarse grid code ('*_F' reprendents a subroutine name)

3 Preliminary results of the nesting POM

We verified nesting effects about some examples, namely, unstable front and flow over a seamount and response of jet to strong wind stress. Three experiments are performed and compared for each test. They are coarse grid experiment (CGE), fine grid experiment (FGE) and nested grid experiment (NGE). In all test cases salinity is constant (35 psu), f-plane is used and a nesting ratio M is 3.

In first test case(unstable front) difference between one-way nesting and two-way nesting is particularly examined. In second case(seamount problem) we show treatment of different topography between CGE and NGE and check stability of nesting calculation. Moreover two feedback methods from nested grid to coarse grid are discussed.

In third case (response of jet to strong wind stress) difference of upwelling/downwelling pattern among experiments is investigated.

3.1 Test 1 : unstable front

We show results of unstable front and meander as first test case for our nesting code. We refer to Wang (1993)[16] 's single grid experiment and Oey (1996) [8] 's nested grid experiment. The model basin is f-plane ($f = 9.37 \times 10^{-5} 1/s$) and 48km (east-west, x-direction) × 68km (north-south,y-direction) square re-

gion. Depth of the model is constant (200m). Periodic boundary condition is imposed at northern and southern side. Half-slip and zero normal flow are imposed at eastern and western side. The surface forcing is zero and quadratic bottom stress with a drag coefficient of 2.5×10^{-3} is used.

Grid resolution and time step of each grid is shown in Table 1. There are 6 equally-spaced sigma levels for each grid.

Table 1 Grid resolution and time step of test 1

	CGE	FGE,NGE
horizontal grid spacing	4km	4/3km
external time step	15s	5s
internal time step	15×30s	5×30s

Horizontal viscosity coefficients are determined by Smagorinsky type formula proportional to the horizontal grid size and the total deformation rate (Mellor (1996)[10]). The proportional coefficient is chosen to be 0.2.

Initial state of the single grid experiment (CGE and FGE) is y-independent basic temperature profile

$$T=18(deg.C)+2(1-tanh((x-48(km)/2)/4(km))\exp(-z/80(m))(5)$$

with zero velocity. The variables of the nested grid are initialized using 10th day result of the CGE.

Meander of temperature front develops from 10th day to 20th day because of baroclinic instability (Wang (1993)[16]) due to round off error. Figure 4 compares the developed meander of each grid at 20th day. FGE (Fig. 4, middle panel) shows stronger amplified meander than CGE (Fig. 4, left panel). NGE shows strong amplified meander as well as FGE. The shape of meander seems to depend on position and area of the nested grid. Figure 5 compares the one-way nesting result and the two-way nesting result. The one-way nesting result (Fig. 5, left panel) resembles the CGE result (Fig. 4, left panel). The meander amplified in the nested area effects on itself due to the periodic boundary condition, namely upstream boundary condition for the nested area.

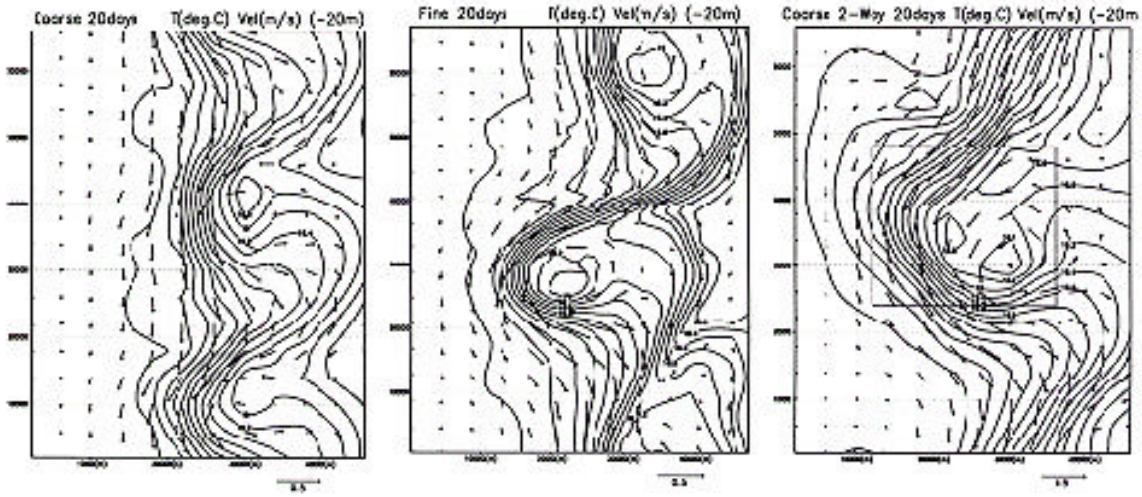

Fig. 4 Horizontal velocity (u, v) and temperature at z = -20m at 20th day, (left panel : coarse, middle panel : fine, right panel : nest) The square region in the right panel shows the nested area.

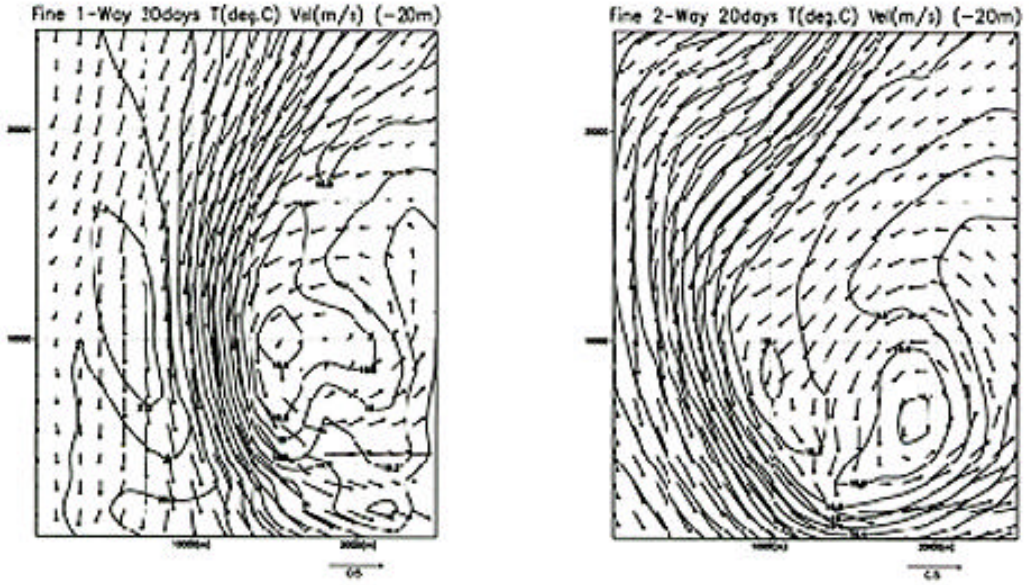

Fig. 5 Horizontal velocity (u, v) and temperature at z=-20m at 20th day in the nested grid, (left panel : one-way, right panel : two-way)

3.2 Test 2 : flow over a seamount

Flow over a steep seamount (Huppert and Bryan (1976)[17]) with 4000m height that is not resolved in coarse grid due to the pressure gradient error in sigma coordinate (Mellor et al. (1994)[18]) is examined.

The model basin is f-plane (f=1.0 × 10^{-4}1/s) and a 340km ×340km square region. The maximum depth of the mode basin is 4500m. A steep seamount is put on the center of the model basin. The height H (x, y) of the seamount is specified as follows.

$$H(x,y) = h_0 - h_m \exp\left[-\left((x - x_c)^2 + (y - y_c)^2\right)/L^2\right]$$
$$h_0 = 4500m,\ L = 25\text{km} \qquad (6)$$

where (x_c, y_c) is the center position of the model basin and h_m is the maximum height of the seamount. Inflow/outflow (barotropic flow, 0.2m/s) boundary condition is imposed at eastern and western side. Half-slip and zero normal flow are imposed at northern and southern side. The surface forcing is zero. The bottom stress is calculated by the quadratic stress formula with the empirical drag coefficient and minimum value of the drag coefficient is 2.5 × 10^{-3} (Mellor (1996)[10]).

Grid resolution and time step of each grid are shown in Table 2. There are 21 sigma levels for each grid with log distributions at the top and bottom and with a linear distribution between 6th levels and 19th levels.

Table 2 Grid resolution and time step of test 2

	CGE	FGE,NGE
horizontal grid spacing	8km	8/3km
external time step	10s	10/3s
internal time step	10×30s	10/3×30s

Horizontal viscosity coefficients are determined by the same Smagorinsky type formula as the first case (section 3.1). The proportional coefficient is chosen to be 0.2.

Initial state of the single grid experiment (CGE and FGE) is xy-independent basic temperature profile

$$T = 5\ (deg.C) + 15\exp\left(-z/1000\ (m)\right) \qquad (7)$$

with uniform speed 0.2m/s of barotropic velocity. The initial state of the nested grid is interpolated from the initial state of the coarse grid.

The coarse grid (horizontal resolution 8km) can treat a seamount with 3300m at most. But it can not treat seamount with 4000m (see Fig. 6). Namely the seamount with 4000m discretized in grid of 8km spacing can not satisfy the empirical condition by Mellor et al. (1994)[18]

$$S \equiv \frac{\left|H_1 - H_2\right|}{H_1 + H_2} \leqq 0.2 \qquad (8)$$

where H_1 and H_2 represent depths of arbitrary adjacent cells and S is called slope parameter by Mellor et al. (1994)[18] . The slope parameter S can be considered as an indication to estimate the pressure gradient error in sigma coordinate (Mellor et al. (1994)[18]) in permitted range. The slope parameter S and the pressure gradient error in sigma coordinate are smaller estimated for smaller grid spacing when the same bottom topography is used. The fine grid spacing of 8/3 km can resolve the seamount with 4000m in this sense. Two-way nesting with the nested grid (horizontal resolution 8/3km) that an resolve this steep seamount makes possible to treat the steep seamount.

Subroutine 'AJSTH\F1' (see Fig. 3) allows steep topogra-

phy in the overlap region of coarse grid. Coarse grid depth in the overlap region is averaged from nested grid depth. It is not necessary to satisfy the Mellor's empirical condition (8) for the coarse grid spacing in the overlap region of coarse grid. Nested grid topography is determined so that the depth satisfies the Mellor's empirical condition (8) for fine grid spacing. Topography of fine grid near the input interfaces is adjusted so that it is coincident with topography of coarse grid.

Figure 7 compares subsurface (-420m) temperature and horizontal velocity of each grid experiment. Warm anomaly drifting downstream and cold anomaly remaining over the seamount of NGE are represented more similar to anomalies of FGE than anomalies of NGE.

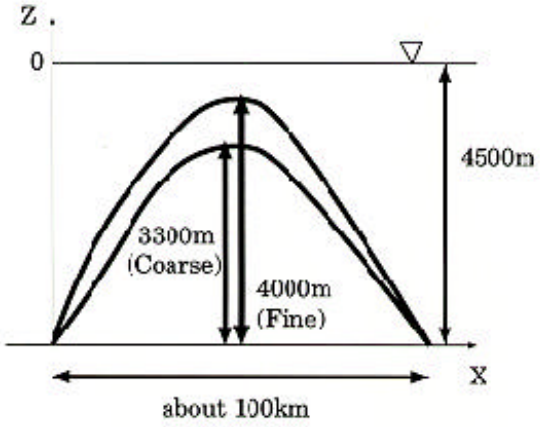

Fig. 6 Steep seamount configuration

Table 3 shows that the two-way nesting has achieved significant reductions of memory and CPU time. Generally if horizontal grid spacing becomes 1/M times smaller than CGE grid spacing, necessary memory size becomes M^2 times larger than CGE and CPU time becomes M^3 times larger than CGE. In this case $M = 3$. Table 3 represents that the nested grid effectively saves computer resources.

Table 3 Comparison of computational performances on the Silicon Graphics Origin 2000

	CGE	FGE	NGE
Memory size	5.5 Mb.	45.0 Mb.	11.7 Mb.
time for 10days	11 min.	340 min.	71 min.

(compile option involves '-O3', 2 PE calculation)

295 days run was performed to check computational stability. Figure 8 shows temporal variation of domain averaged temperature for the coarse grid and that for the nested grid in NGE. Temperature variation is within the range of 0.002 deg. C for the coarse grid and 0.02 deg. C for the nested grid at most. The other variables (velocity, sea surface height, etc.) are also within the reasonable range (not shown) and the pattern of warm/cold anomalies at 295th day is almost the same as that at 10th day shown in Fig.7. Therefore the nesting calculation for the seamount problem is stable.

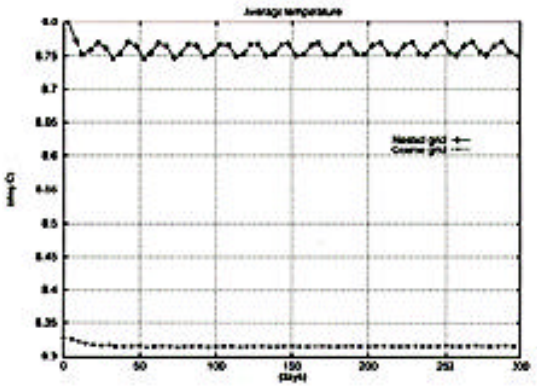

Fig. 8 Domain averaged temperature for 295 days run of NGE

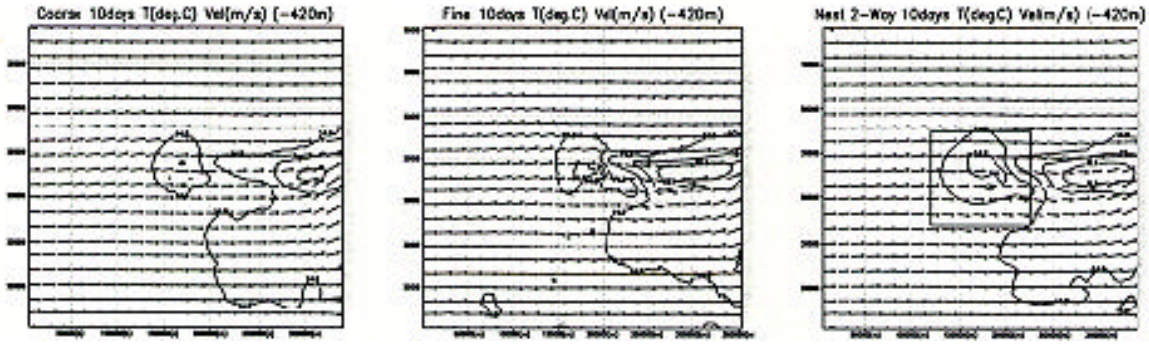

Fig. 7 Horizontal velocity (u, v) and temperature at z = -420m at 10th day, (left panel : coarse, middle panel :fine, right panel: nest) The square region in the right panel shows the nested area.

Sensitivity of fine grid value averaging methods on a coarse grid point for making coarse grid topography in the overlap region and for two-way feedback process also has been investigated. In standard case experiment averaging method is simple as shown in equation (3) and (4),

$$X^c_{I,J} \equiv \frac{1}{9}\left(\begin{array}{l} X^n_{i-1,j+1} + X^n_{i,j+1} + X_{i,j+1} + X^n_{i-1,j} + X^n_{i,j} \\ + X_{i+1,j} + X^n_{i-1,j-1} + X^n_{i,j-1} + X^n_{i+1,j-1} \end{array} \right) \quad (9)$$

where $X^c_{i,j}$ denotes a coarse grid value and $X^n_{i,j}$ denotes a nested grid value in a corresponding coarse grid cell. In second case experiment averaging method is the Shapiro filter (Shapiro (1970)[19) ; Zhang et al. (1986) [5)]) given by

$$\begin{array}{l} X^c_{I,J} \equiv \\ 1/4 X^n_{i,j} + 1/8\left(X^n_{i+1,j} + X^n_{i-1,j} + X^n_{i,j-1} + X^n_{i,j+1} \right) \\ + 1/16\left(X^n_{i+1,j+1} + X^n_{i+1,j-1} + X^n_{i-1,j+1} + X^n_{i-1,j-1} \right) \end{array} \quad (10)$$

Moreover fine grid depth is identical with coarse grid depth at coincident point in the overlap region in this experiment. The results of two experiments seem almost same (not shown).

3.3 Test 3 : response of jet to strong wind stress

We applied the developed nesting POM to a simulation of response of an idealized Kuroshio to strong head wind due to Typhoon (Miyazawa and Minato (1999) [9)]) in presence of an idealized cape regarded as Cape Shionomisaki, the southernmost tip of the Kii Peninsula.

The model basin is f-plane (0.8×10^{-4}1/s) and a square region, 360*km* wide and 600*km* long in west-east extent that idealizes coastal ocean off Shikoku Island and the Kii Peninsula. The maximum depth is 4000*m*. The basin has a continental shelf-slope that extends from the northern coast to 100km distance . Half-slip and no normal flow are imposed on the northern boundary. Distance between jet and coast is a parameter for experiments. The western, eastern and southern boundaries are treated as the open boundaries. Along the open boundary, a radiation condition (Mellor, 1996) is adopted on velocities and one-sided advection is adopted on tracer variables. The horizontal viscosity/diffusivity and the empirical drag coefficient for the bottom stress are gradually increased near the eastern boundary in order to form stable jet. The bottom stress is calculated by the quadratic stress formula with the empirical drag coefficient and minimum value of the drag coefficient is 2.5×10^{-3} (Mellor, 1996).

The current of the model Kuroshio is driven by inflow on the western boundary and outflow on the eastern boundary. The velocity profile $u(y, z)$ of the inflow/outflow consists of geostrophic current calculated from the basic density profile $\rho(y, z)$ with the reference level of 1800*m* and barotropic component u_{bt}.

$$u(y,z) = \left\{ \begin{array}{c} \frac{g}{f_{\rho 0}} \int_{-1800(m)}^{z} \frac{\partial \rho}{\partial y} dz + u_{bt} \\ \left(-1800(m) \leqq z \leqq 0(m) \right) \\ u_{bt} \quad \left(-400(m) \leqq z \leqq -1800(m) \right) \end{array} \right\} \quad (11)$$

Total volume transport is 25*sv*. The barotropic velocity component u_{bt} is given on the model Kuroshio, in $247.5km \leqq y \leqq 267.5km$.

$$u_{bt} = \frac{1}{20(km) \times 4(km)} \left(25(sv) - \frac{g}{f_{\rho 0}} \int_0^{Ly} \int_{-1800(m)}^{0} \int_{-1800(m)}^{z} \frac{\partial \rho}{\partial y} dz' dz dy \right) \quad (12)$$

The basic temperature $T(y, z)$ is given by

$$T(y, z) = 18.\,(deg.\,C) + \Delta T \exp(z/D(y)) \quad (13)$$

where ΔT that determines intensity of stratification is 5(*deg.C*). The main thermocline depth $D(y)$ is specified by

$$D(y) = \frac{1}{2}\Delta D\left(1 - \tanh\left((y - y_0)/W_f \right) \right) + D_{min} \quad (14)$$

$$\Delta D = 400m,\ y_0 = 257.5km$$
$$D_{min} = 100m,\ W_f = 10km$$

where y_0 is a position of the axis of the Kuroshio ; W_f is a width of the temperature front. The thickness of the idealized Kuroshio $D_{min} + \Delta D$ is 500 *m* and the coastal thermocline depth D_{min} is 100*m*. Initial temperature and velocity profiles are x-independent and they are the same profiles as the inflow boundary conditions.

Grid resolution and time step of each grid are shown in Table 4. There are 21 sigma levels. Minimum grid spacing is 0.5% at the surface. Maximum grid spacing is 15% in the middle levels. The horizontal viscosity is constant. The horizontal diffusivity is the same value as the horizontal viscosity. Value of the horizontal viscosity/diffusivity is 200 (m^2/s)

Table 4 Grid resolution and time step of test 3

	CGE	FGE,NGE
horizontal grid spacing	5km	5/3km
external time step	6s	2s
internal time step	6×30s	2×30s

After 50days calculation without wind stress, quasi-equilibrium jet is formed corresponding to the specified inflow/outflow conditions. The easterly wind stress ($10\,dynes/cm^2$) is applied from 50th day to 55th day for 5 days. The magnitude of wind stress is constant over the whole domain. Any heat and flesh water surface flux is not applied. Total 60 days calculation is performed.

CGE, FGE and NGE are performed in order to investigate dependency of grid resolution and effect of the nesting POM. We used the coarse grid result at 50th day (the beginning of the wind event) to initiate the nested grid experiment. The nested grid experiment was performed from 50th day to 60th day. We also found that Kurihara an Bender (1980)[4]'s damping scheme for temperature calculation at the eastern and western input interface points in the nested area given by

$$\frac{\partial T}{\partial t} = \cdots\cdots - \frac{\left(T - \overline{T}\right)}{T_d} \qquad (15)$$

reduces the noise of temperature near the nest boundary in this problem as well as Oey (1996)[8] 's experiment that treats coastal upwelling due to wind stress. T_d in the scheme (15) is the damping time (600s). $\overline{T}$ is the average of two point values on either side of the point being adjusted and along the line normal to the interface.

Figure 9 shows horizontal velocity (u, v) and temperature at z = -100 m level after 7 days from the beginning of the wind event. The warm water intrudes into coastal region of the downstream side along the cape. This feature is shown in Fig. 9, all panels. Downwelling near the cape due to closeness of the Kuroshio (Miyazawa and Minato (1999)[9]) in front of the cape and subsequent advection of the downwelling warm water by mean flow cause the intrusion of the warm water.

We compare the results of three experiments shown in Fig. 9. All cases show the similar warm water intrusion into the downstream side along the cape. The nested grid experiment (Fig. 9, lower panel) shows that the upwelling region(cold anomaly) is extended along the offshore side of the Kuroshio axis. The fine grid experiment (Fig. 9, middle panel) shows that the upwelling region is also extended along the offshore side of the Kuroshio axis. The coarse grid experiment (Fig. 9, upper panel) shows that the upwelling region is extended along the offshore side of the Kuroshio axis in the only upstream region. Because the fine grid allows stronger amplification of meander due to instabilities than the coarse grid,downwelling/upwelling is intensified due to the stronger shear of the Kuroshio than the coarse grid experiment. Figure 10 shows vertical velocity after 4 days from the beginning of the wind event, at the last time of the wind event. The fine grid result (Fig. 10, middle panel) shows more intensified downwelling/upwelling patterns than the coarse grid result (Fig. 10 upper panel). The nested grid result (Fig. 10, lower panel) also shows intensified downwelling/upwelling patterns in the nested area as well as the fine grid result.

We performed other experiment using another nesting grid that is composed of 15km coarse grid and 5km grid. But deformation of the Kuroshio due to strong wind stress was weaker than the above 5km coarse grid and 5/3km nested grid experiment, because downwelling/upwelling causing deformation of the Kuroshio depends on the shear of the Kuroshio (Miyazawa and Minato (1999)[9]). We found that 15km coarse grid and 5km grid can not represent the strong shear of the Kuroshio.

4 Summary

The developed two-way nesting code for the Princeton Ocean Model (POM) was applied to the some problems such as unstable front, flow over a seamount and response of jet to strong wind stress. Our two-way nesting POM code could simulate more detailed features than the coarse grid results and reduce computer resources compared with the fine grid results.

It is still necessary to examine basic properties of nesting, for example, permeability of fundamental waves, conservation of physical quantities, sensitivity for the nesting ratio and comparison with the variable grid spacing. On the other hand, our nesting code for the POM will be applied to actual problems in coastal ocean modelling. We hope that our nesting code for the POM will show its availability in various problems.

Acknowledgment

The authors express their sincere thanks to Prof. T. Yamagata for his useful advice.

References

1) Kagimoto, T. and T. Yamagata : Seasonal transport variations of the Kuroshio : An OGCM simulation. J. Phys. Oceanogr., **27**, 403-418. (1997)

2) Mitsudera, M., Y. Yoshikawa, B. Taguchi and H. Nakamura : High-resolution Kuroshio/Oyashio System Model : Preliminary Results. JAMSTECR, **36**, 147-155. (in Japanese with English Abstract) (1997)

3) Guo X., Y. Miyazawa, H. Hukuda and T. Yamagata : Volume transport through the straits of Japan/East seas-Preliminary results from a nested ocean model for Japan Coastal Ocean Predictability Experiment (JCOPE). Proc. CREAMS' 99 Intl Sympo. (1999)

4) Kurihara, Y. and M. A. Bender : Use of a movable nested-mesh model for tracking a small vortex. Mon. Wea. Rev., **108**, 1792-1809. (1980)

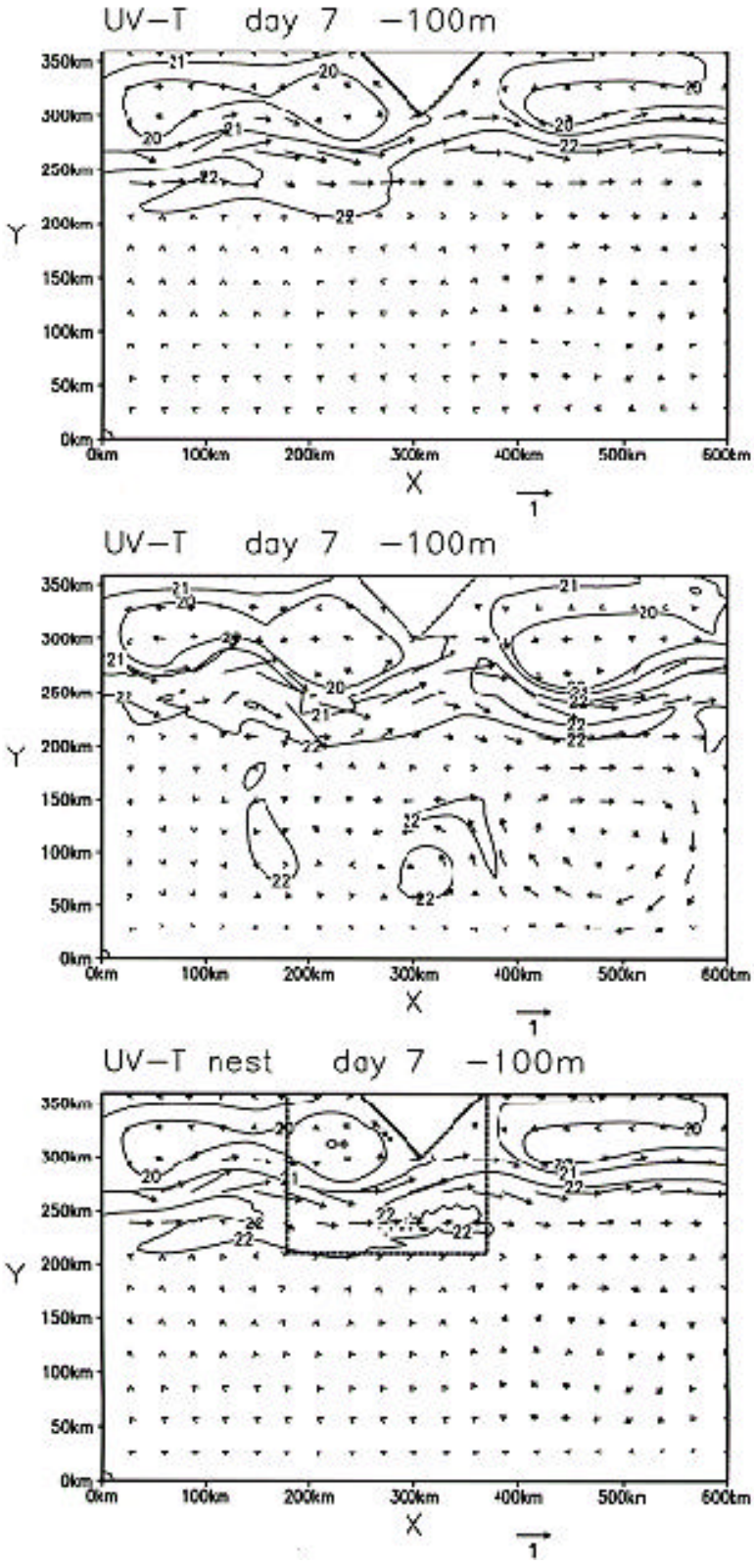

Fig. 9 Horizontal velocity (u, v) and temperature at z = -100m level after 7 days from the beginning the wind event (upper panel : coarse, middle panel : fine, lower panel : nest) The square region in the right panel shows the nested area

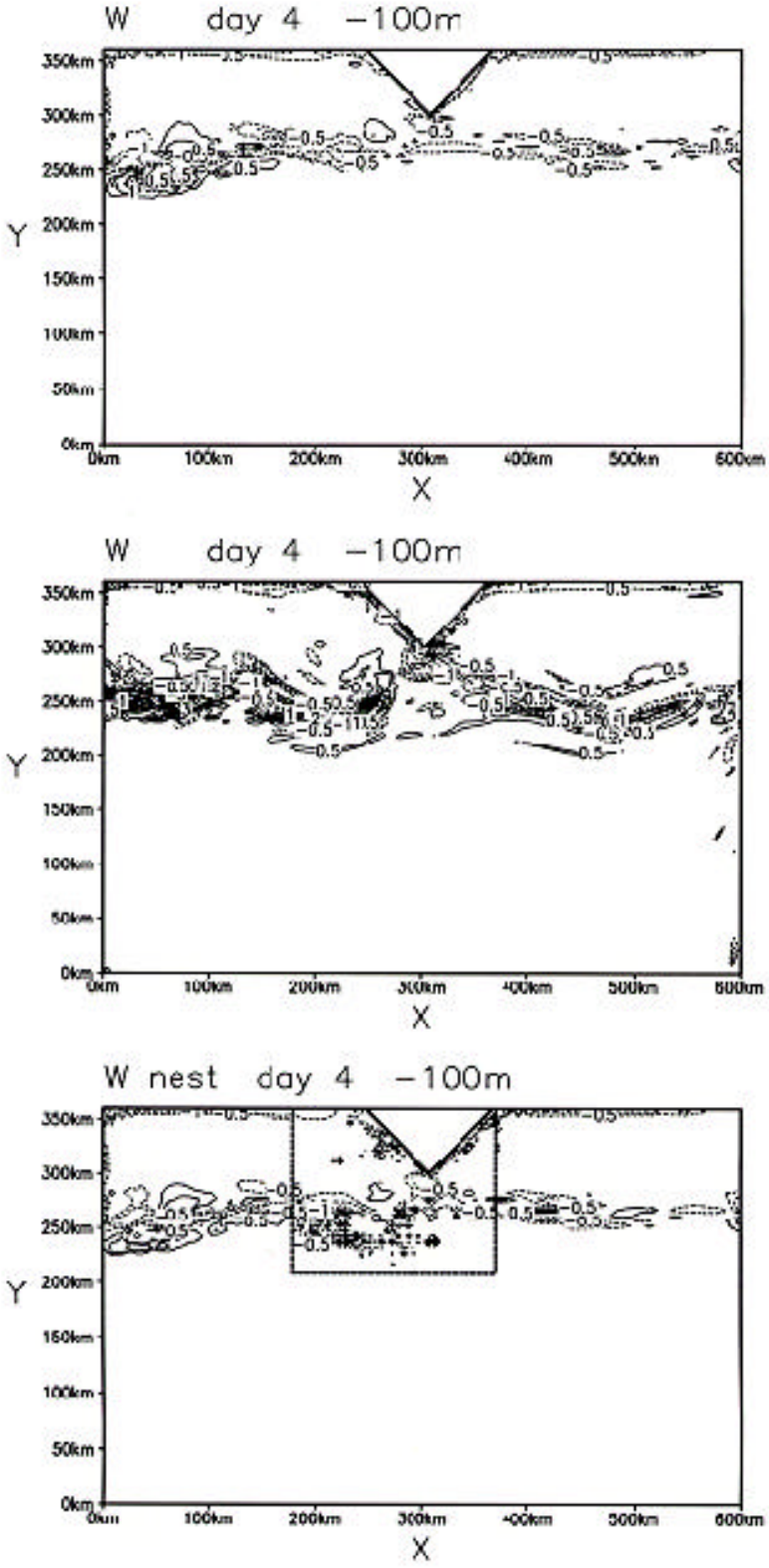

Fig. 10 Vertical velocity w at z = -100m level after 4 days from the beginning the wind event, (left panel : coarse, middle panel : fine, right panel : nest) The square region in the right panel shows the nested area

5） Zhang, D. L., H. R. Chang, N. L.. Seaman, T. T. Warner and J. M. Fritsch : A two-way interactive nesting procedure with variable terrain resolution. Mon. Wea. Rev., **114**, 1330-1339. (1986)
6） Spall, M. A. and W. R. Holland : A nested primitive equation model for oceanic applications. J. Phys. Oceanogr., **21**, 205-220. (1991)
7） Oey, L. -Y., and P. Chen : A nested-grid model : with application to the simulation of meanders and eddies in the Norwegian coastal current. J. Geophys. Res., **97**, 20063-20086. (1992)
8） Oey, L. -Y. : The accuracy of a nested-grid ocean model. preprint. (1996)
9） Miyazawa Y. and S. Minato : Kuroshio damping phenomenon caused by a strong wind using POM and a two-way nesting POM., accepted by Journal of Oceanography. (1999)
10） Mellor, G. L. : Users guide for a three-dimensional, primitive equation, numerical ocean model. Princeton University. (1996)
11） Minato S. : Storm surge simulation using POM and a revisitation of dynamics of sea surface elevation short-term variation. Papers in Meteor. and Geophys., **48**, 79-88. (1998)
12） Hong, C. H. : Simulation of sea water response in Deukryang Bay to typhoon using Princeton Ocean Model. J. Korean Soc. Oceanogr., **33**, 53-63. (1998)
13） Asselin, R. : Frequency filters for time integration. Mon. Wea. Rev., **100**, 487-490., (1972)
14） Mellor, G. L., and T. Yamada : Development of a turbulence closure model for geophysical fluid problems. Rev. Geophys. Space Phys., **20**, 851-875. (1982)
15） Mellor, G. L. : An equation of state for numerical models of oceans and estuaries. J. Atmos. Oceanic Tech., **8**, 609-611. (1991)
16） Wang, D. -P. : Model of frontgenesis: subduction and upwelling. J. Mar. Res., **51**, 497-513. (1993)
17） Huppert, H. E. and K. Bryan : Topographically generated eddies. Deep Sea Res., **23**, 655-679. (1976)
18） Mellor, G. L., T. Ezer, and L. -Y. Oey : The pressure gradient conundrum of sigma coordinate ocean models. J. Atmos. Oceanic Tech., **11**, 1126-1134. (1994)
19） Shapiro, R. : Smoothing, filtering and boundary effects. Rev. of Geophys. Space Phy., **8**, 359-387. (1970)

（原稿受理：1999 年 6 月 9 日）